

# Removing Organic Dye by Cellulose Acetate Nanocomposite Membrane Ultrafiltration: Effect of Bio-Nanoparticle Size

**Missaoui, Takwa\*<sup>+</sup>**

National Agronomy Institute of Tunis, 43 Avenue Charles Nicolle, 1082 Tunis, TUNISIA

**Elboughdiri, Noureddine<sup>•</sup>**

Chemical Engineering Department, College of Engineering, University of Ha'il, P.O. Box 2440, Ha'il 81441, SAUDI ARABIA

**Imran Khan, Muhammad**

Research Institute of Sciences and Engineering, University of Sharjah, Sharjah, 27272, UNITED ARAB EMIRATES

**Ghernaout, Djamel<sup>••</sup>**

Chemical Engineering Department, College of Engineering, University of Ha'il, P.O. Box 2440, Ha'il 81441, SAUDI ARABIA

**Girigoswami, Agnishwar**

Medical Bionanotechnology, Faculty of Allied Health Sciences, Chettinad Hospital & Research Institute (CHRI), Chettinad Academy of Research and Education, Kelambakkam, Chennai-603 103, INDIA

**Sami, Rokayya**

Department of Food Science and Nutrition, College of Sciences, Taif University, P.O. Box 11099, Taif 21944, SAUDI ARABIA

**ABSTRACT:** This work reported a new perspective on improving the green synthesis of titanium dioxide (TiO<sub>2</sub>) nanoparticles (NPs) from Aloe vera plant leaf extract and their incorporation into membranes for several applications. The X-ray diffraction of the powder depicted that the size of the samples TiO<sub>2</sub> NPs (1 h) and TiO<sub>2</sub> NPs (5 h) were  $83 \pm 15$  (Ø2) nm and  $23 \pm 1.6$  nm (Ø1), respectively. With two sizes of TiO<sub>2</sub> NPs as an additive, cellulose acetate (CA) membranes and a series of TiO<sub>2</sub>/CA hybrid membranes were prepared using a phase-inversion method. The membrane characterization was carried out by Fourier transform-infrared spectroscopy, scanning electron microscope (SEM), water content, contact angle, porosity, and pure water flux measurements. The cross-section SEM

---

\* To whom correspondence should be addressed.

+ E-mail: Takwamissaoui728@yahoo.com

• Other Address: Chemical Engineering Process Department, National School of Engineers Gabes, University of Gabes, Gabes 6029, TUNISIA

•• Chemical Engineering Department, Faculty of Engineering, University of Blida, P.O. Box 270, Blida 09000, ALGERIA  
1021-9986/2023/5/1512-1527 16/\$/6.06

images indicated that the size of macro-voids was reduced and the width of the membrane pores was slightly increased by the addition of  $\text{TiO}_2$  ( $\text{\AA}$ 1). Membrane performance has been investigated in terms of dye Remazol Brilliant Red F3B (Reactive Red 180, RR 180) removal, which could be, however, affected by the competitive effect of another chemical species present in the solution such as NaCl salt. Indeed, NaCl decreased the retention rate of dye due to electrostatic interactions, as the chloride ions compete with the anionic dye molecules during the complexation process. The retention rate decreased at alkaline pH due to interaction forces between the membrane surface and anions of the RR 180.

**KEYWORDS:** Cellulose acetate (CA); Titanium oxide ( $\text{TiO}_2$ ); Nanoparticles (NPs); Aloe vera; Hybrid membrane; Azo dye treatment.

## INTRODUCTION

Industrial dye effluents have long been recognized as a significant source of water contamination. They constitute a wide family of organic pollutants known for their harmful effects on the environment and human health. The treatment of effluent azo dyes has gained considerable attention [1-3]. Separation procedures such as coagulation/flocculation and sedimentation (or sedimentation) are utilized in the traditional treatment of textile industry wastewater. However, all of them require a final disposal, maybe with preceding on-site storage. The disadvantages of such chemical techniques include the use of extra chemicals, greater sludge generation, and the requirement to remove additional color and chemical oxygen demand. In some textile facilities, unconventional membrane separation is used in conjunction with specific pre-treatment processes [4]. Membranes are commonly used in chemical technology and have been used in a wide variety of applications, such as the manufacture of high-quality water, the removal or recovery of hazardous or useful materials from various industrial effluents, food and pharmaceutical applications. Separation, concentration, and purification have become industrially viable unit operations with the advent of membrane technology thanks to high separation performance, low operating energy, and ease of operation with modern compact modules of several types [5].

Cellulose Acetate (CA) is very common, like most of various polymeric materials used to prepare phase-inversion membranes. CA offers several features such as good durability, high biocompatibility, good desalination efficiency, high potential flux, and relatively low-cost [5-7]. It has already been widely used for reverse osmosis,

microfiltration, and gas separation [8,9]. Also, CA membranes have excellent hydrophilicity, which is very important in the minimization of fouling phenomenon [6,10].

Nevertheless, there are drawbacks related to these two strategies, such as poor permeate flow, high costs and low selectivity. In order to deal with such obstacles, organic-inorganic hybrid membranes have been suggested. Such hybrid membranes are created by adding micrometer and nanometer sizes of inorganic oxide particles to the polymeric casting solution or by producing them *in situ* [11-13]. Few scholars have identified organic polymer mixing with inorganic materials such as alumina, titanium, silica, etc. [14-16]. NanoParticles (NPs) have been used in membrane preparation for two main purposes. Due to interactions between the surface of NPs and polymer chains and/or solvents during membrane preparation, one creates membranes with a desirable structure. These structural changes result in favorable gas separation selectivity and permeability and adequate performance in membranes for ultrafiltration (UF) and nanofiltration. The other objective is to regulate membrane fouling triggered by functional groups of NPs and their hydrophilic properties [17-20]. The existence of the inorganic phase can also be used to restrict the molecular movements of the polymer chains and improve the mean distance between the polymer chains (free volume). Simultaneous improvement of membrane porosity, stability and performance can result from limited molecular motions and a favorable increase in the mean distance between chains [21].

Li et al. [15] prepared blend membranes based on polyethersulfone (PES) and titanium oxide ( $\text{TiO}_2$ ) materials by phase inversion process and found that

the addition of TiO<sub>2</sub> particles to the polymer casting solution resulted in higher thermal stability. The permeation properties of the hybrid membranes were significantly superior to the pure PES membrane and the mean pore size is also enhanced with the addition of TiO<sub>2</sub> NPs.

In the recent years, many researchers have examined the preparation of TiO<sub>2</sub> nano-inorganic mixed matrix membranes from two ways such as assembling engineered NPs on the surface of the porous membranes [15,22,23] or mixing them with polymeric casting solution [5,24,25].

Both of the cross-linking degree of the polymeric matrix and the types of attachment bonds between the polymer chains and inorganic phases in the composite fabric will influence the structure of the membranes [26,27]. Through this point of view, we have concentrated on the production of low-cost, inorganic membranes, having a satisfactory yield and good performance as a principal feature.

Recently, biosynthesis or green synthesis emerges as an alternative process for NPs preparation. The benefit of plant extracts is providing a biological synthesis route of several NPs. Such synthesis route is more environmentally friendly, cost-effective, biocompatible, safe, and gives a regulated synthesis with defined size and morphology of NPs. There is no obligation to add different chemical stabilizers, since the extract is combined with the salt solution as the precursor and the plant extract acts as a reducing and stabilizing agent for the synthesis of NPs [28].

In this study, an eco-friendly and rapid method for synthesis of TiO<sub>2</sub> NPs was described. At the best of our knowledge, this is the first time that a study attempts to exploit the *Aloe vera* leaves extract as reducing agent in the green synthesis of TiO<sub>2</sub> NPs. The aim of this work is to improve the performance of CA membranes by adding two sizes of TiO<sub>2</sub> NPs in the polymeric dope solution. Therefore, the effects of TiO<sub>2</sub> NPs on the structure of the CA composite membrane were evaluated. Membrane performance was evaluated in terms of water permeability. Also, CA composite and CA control membranes have been fully featured based on morphology (scanning electron microscopy, SEM), contact angle, porosity, Fourier transform-infrared (FT-IR) spectroscopy and equilibrium water content. Then, the separation performance of resulting membranes was investigated by soluble dye removal (Red Brilliant F3B (RR 180)). In addition, various operating conditions such as transmembrane pressure, pH

solution, concentrations of dye and amounts of added NaCl were tested.

## EXPERIMENTAL SECTION

### Materials

A model azo dye, Remazol Brilliant Red F3B (Reactive Red 180, RR 180), obtained from Dystar, was used without further purification. Further, CA (approximately 39.8% acetyl content) was procured from Sigma-Aldrich (CAS 9004-35-7). It was with an average molecular weight of 30,000 g/mol and used as the polymer forming membrane. Further, dimethylformamide (DMF) (CAS 68-12-2) and polyethylene glycol (PEG 1000) (CAS 25322-68-3) were supplied from Dae-Jung chemicals.

The pH of the solution was kept at intended pH values (pH = 2-10) by the addition of HCl (0.1 M) and NaOH solution (0.1 M). The water used for all prepared solutions is distilled water, and all experiments were conducted at room temperature.

### Synthesis of titanium oxide (TiO<sub>2</sub>) nanoparticles (NPs)

*Aloe vera* plant leaves were collected from Kasserine (Tunisia) on the beginning of spring. Herbarium code number: TN-65118. The leaves of *A. vera* were separated from plant and thoroughly washed and cut into small pieces. Then, 25 g of the leaves were put into 100 mL of distilled water and boiled for 2 h at 90°C. After that, the mixture was filtered through Whatman No.1 filter paper and stored at 4°C for the synthesis of NPs.

TiO<sub>2</sub> NPs were prepared using TiCl<sub>4</sub> as a precursor. Briefly, 100 mL of leaves extract were added dropwise to a 100 mL 1.0 N TiCl<sub>4</sub> solution in deionized water. The leaf extract present in solution mixture act as a capping/stabilizing agent to prevent agglomeration and achieve the desired shape and size of the TiO<sub>2</sub> NPs. The mixture was kept under constant stirring for 4 h at room temperature and neutral pH. The obtained white suspension was filtered using Whatman No.1 filter paper to separate the formed NPs, which were then washed with double distilled water repeatedly to remove the by-products.

Upon subsequent heating at 100°C, the formation of TiO<sub>2</sub> took place due to the condensation process. The obtained dry powder was further calcined at 500°C for the duration of the calcination of 1 h (Ø2) and 5 h (Ø1) to decompose all biomolecules; at a such high temperature, there were only the stable metal oxide NPs that are retained [29].

The mechanism behind the formation of TiO<sub>2</sub> NPs was hydrolysis of Titanium-isopropoxide [30].

#### **Analysis of titanium oxide (TiO<sub>2</sub>) nanoparticles (NPs)**

The TiO<sub>2</sub> NPs powders were characterized by various techniques to specify their structural and textural properties. The crystalline phase was analyzed by X-ray diffraction (XRD). XRD data were collected on an X'Pert Pro Panalytical diffractometer with CuK $\alpha$  radiation ( $\lambda = 0,15406$  nm) and graphite monochromatic. The XRD measurements were performed using a phase scanning method (range from 10 to 85), the scanning rate was  $0.02\text{ s}^{-1}$  and the step time was 1s. The infrared (IR) spectrum has been registered by a Perkin-Elmer (FT-IR 2000) spectrometer using KBr pellets in the region of 4000-400  $\text{cm}^{-1}$ . Morphology was tested using Scanning Electron Microscopy (SEM) (Philips XL30 SFEG).

#### **Membrane preparation method**

All the membranes were obtained by a phase inversion process as follows: 0.05 g TiO<sub>2</sub> for each diameter ( $\varnothing 1$  (5 h) and  $\varnothing 2$  (1 h)) were added to dimethylformamide (DMF) solution under rapid stirring. The mixture solution was submitted to ultrasonication and stirred for 3 hours. Then 4 g of cellulose acetate (CA) was added to each mixture under stirring, and the mixture was again stirred for 72 hours at 70°C. Approximately 1 g of the pore-forming reagent (i.e., PEG-1000) was added to each mixing solution and agitation was maintained for 12 h at 70°C to obtain the casting suspension. The casting suspension was held static for 24 h at 70°C to remove the gas bubbles prior to use. The casting suspension was casted with a casting knife onto a glass plate at  $25\pm 1^\circ\text{C}$ . The nascent membrane was evaporated at  $25\pm 1^\circ\text{C}$  for 15 s in air and then immersed in a deionized-water precipitation bath maintained at  $15\pm 1^\circ\text{C}$ . For all prepared membranes, after complete precipitation, the membrane was transferred to a drip-washing water bath for 3 days at room temperature to remove the remaining solvents from the membrane structures. The prepared membranes were then tested [31].

#### **Membrane characterization**

To determine the features of prepared membranes, several characterization techniques were used. The functional groups on the surface of the membrane were identified using FT-IR spectroscopy device with IR

(Model: Perkin Elmer Spectrum RX I). The FT-IR spectra of the membranes were recorded in transmittance mode over a wave number range of 4000 to 500  $\text{cm}^{-1}$  at 25°C.

The images of the membranes were taken with a scanning electron microscope JEOL (Japan Electro Optic Laboratory, model JSM 5400A, Peabody, Massachusetts, USA). The membranes were freeze-fractured in liquid nitrogen to give a generally consistent and clean break and were then sputter coated with a thin film of gold. The images were made at 15 kV with a magnification value (or factor) ranging between 200 and 2,000.

The contact angle is measured as a guide to the hydrophobicity of the membrane. It is determined using a Theta optical blood pressure monitor (Attension) with an automated liquid pumping system. The membrane sample is contacted with a droplet of distilled water of approximately 5  $\mu\text{L}$  through a microliter syringe at room temperature. A light source is placed behind the sample and the contact angle has been calculated using computer software.

The water content of the membranes was obtained after soaking membranes in water for 12 hours; the membranes were weighed followed by blotting with blotting paper. The wet membranes were placed in vacuum drier at 60°C for 2 hours from the dry mass of the membranes. The percentage water content was calculated using Eq. (1):

$$\text{Water content(\%)} = \frac{W_w - W_d}{W_w} \times 100 \quad (1)$$

where:  $W_w$  is the weight of the wet membrane and  $W_d$  is the weight of the dry membrane.

The membrane porosity  $\varepsilon$  (%), defined as the ratio between volume of voids present in the membrane and the overall membrane volume, was measured by gravimetric method as it is reported in the literature [32]. The method consists in weighting the membrane in dry and wet (kerosene for 24 h) conditions. The porosity was calculated according to Eq. (2):

$$\varepsilon(\%) = \frac{\frac{(W_w - W_d)}{\rho_i}}{\frac{(W_w - W_d)}{\rho_i} + \frac{W_d}{\rho_p}} \times 100 \quad (2)$$

Where:  $\varepsilon$  is the membrane porosity (%);  $W_w$  is the weight of the wet membrane;  $W_d$  is the weight of the dry membrane;  $\rho_i$  is the kerosene density (i.e., 0.82  $\text{g/cm}^3$ ) and  $\rho_p$  is the CA density (i.e., 1.28  $\text{g/cm}^3$ ). For each membrane,

three measurements were performed, then the average value and standard deviation were calculated.

The point of zero charge ( $\text{pH}_{\text{PZC}}$ ) can be used to characterize a membrane since it indicates the pH at which the membrane has a zero-surface charge. The determination of  $\text{pH}_{\text{PZC}}$  was performed following the solid addition method [33]. The value of  $\text{pH}_{\text{PZC}}$  can be determined from the curve that cuts the initial pH ( $\text{pH}_i$ ) line of the plot  $\text{pH}_f - \text{pH}_i$  vs.  $\text{pH}_i$  ( $\text{pH}_f$  is the final value of pH).

The main aim of the developed membrane is the dye retention. Given that, the relative charge affinity from dye molecules to membrane surface will play an important role in explaining the rejections obtained, so characterizing the membrane charge will be convenient.

### Filtration application

#### Filtration test

The performance of the prepared membranes was analyzed through a cross-flow system. A schematic diagram of the UF system is shown in Fig. 1. The water permeability,  $L_p$  (L/h  $\text{m}^2$  bar), of the membrane was determined by measuring the permeate flux of distilled water,  $J_w$  (L/h  $\text{m}^2$ ), as a function of transmembrane pressure,  $\Delta P$  (bar), which was varied from 2 to 5 bar. Flux  $J_w$  and permeability  $L_p$  were calculated employing Eq. (3) and Eq. (4), respectively:

$$J_w = \frac{Q}{A \times \Delta t} \quad (3)$$

$$L_p = \frac{J_w}{\Delta P} \quad (4)$$

where:  $Q$  is the quantity of permeate (L);  $A$  is the effective membrane area ( $\text{m}^2$ ); and  $\Delta t$  is the operations time (h).

The rejection experiments for RR 180 were conducted at a transmembrane pressure varying from 2 to 5 bar. The effect of feed pH on dye rejection was studied in the range from pH 2 to pH 10 at a feed concentration of 50 ppm. The effect of ionic strength was determined through varying it from 0.2 to 1 g  $\text{L}^{-1}$ . Also, the effect of dye concentration was investigated from 25 to 75 ppm at their respective natural pH. The rejection  $R$  (%) of dye was calculated using Eq. (5):

$$R(\%) = \frac{1 - C_p}{C_f} \times 100 \quad (5)$$

where:  $C_p$  and  $C_f$  are the concentrations of permeate and feed solutions, respectively.

### Analytical methods

The permeate concentration was measured by ultraviolet (UV)-visible spectrophotometer (Lamba 2, Perkin Elmer) using quartz cells. All measurements were made at the wavelength corresponding to the maximum of absorbance ( $\lambda_{\text{max}}$ ) for dyer 180 that was 540 nm.

## RESULTS AND DISCUSSIONS

### TiO<sub>2</sub> nanoparticles (NPs) characterization

It was discovered that the TiO<sub>2</sub> precursor solution is clear even after the addition of titanium isopropoxide to the water solution, indicating that the metal alkoxide has completely dissolved in the solvent. This transparent solution quickly turns into a slurry with a pale green color with the addition of *A. vera* plant extract, due to the fast reaction of the precursor solution via hydrolysis and condensation produced by the presence of water molecules in *A. vera* plant extract. The color shift demonstrates the encapsulating of TiO<sub>2</sub> particles by a little number of solid biomolecules found in *A. vera* plant extract, and the pale green color grows richer as the concentration of TiO<sub>2</sub> increases.

The structural properties of TiO<sub>2</sub> NPs have been shown by XRD. The TiO<sub>2</sub> (1 h) and TiO<sub>2</sub> (5 h) XRD spectra are depicted in Fig. 2. The observed XRD peaks are in good agreement with the standard JCPDS file (84-1285), which confirmed an anatase structure at all peaks. The favored growth was located along the crystal plane (101). No excess peaks have been observed suggesting that nanocrystals TiO<sub>2</sub> were established at 500°C. The average particle size  $D$  of the samples as prepared was determined using the Debye - Scherrer formula as shown by Eq. (6) [34]:

$$D = \frac{k \times \lambda}{\beta \times \cos \theta} \quad (6)$$

where:  $D$  is the crystallite size (nm);  $\lambda$  is the wavelength (1.5406 Å) of the CuK $\alpha$  radiation used;  $\theta$  is the Bragg angle and  $\beta$  is the full-width at half-maximum that corresponds to the most popular peak (101), both of them are expressed in radians.

The average crystallite size of the TiO<sub>2</sub> NPs is considerably decreased from  $83 \pm 15$  nm to  $23 \pm 1.6$  nm, respectively, with the calcination duration that was increasing from 1 to 5 h. The decrease in particle size with

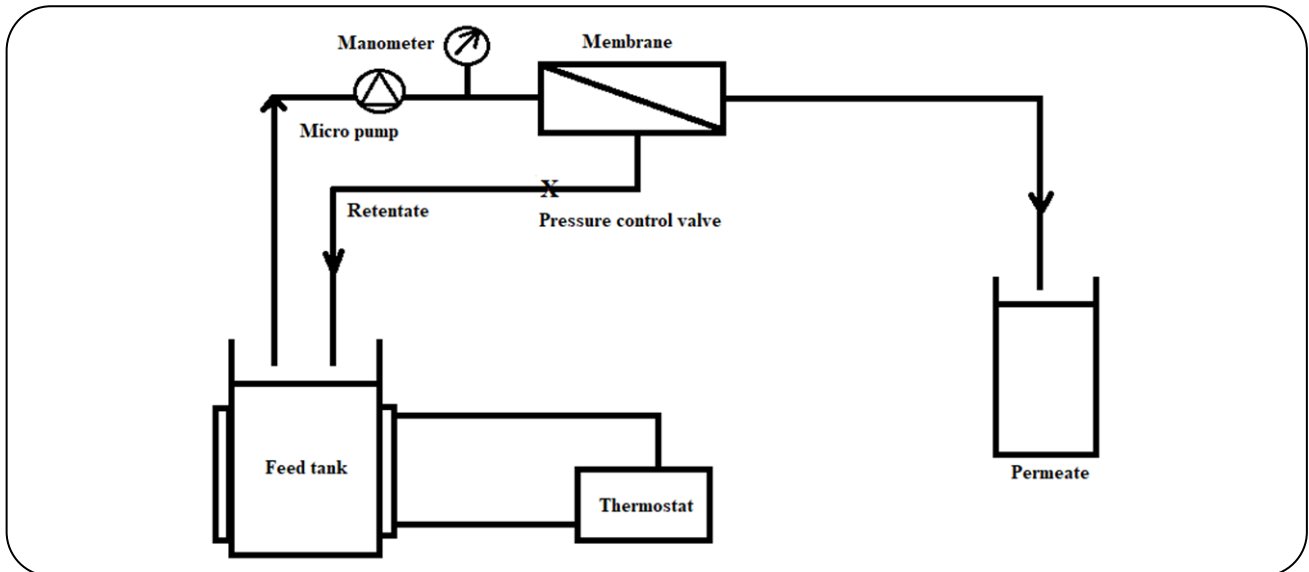


Fig. 1. Schematic of the experimental setup.

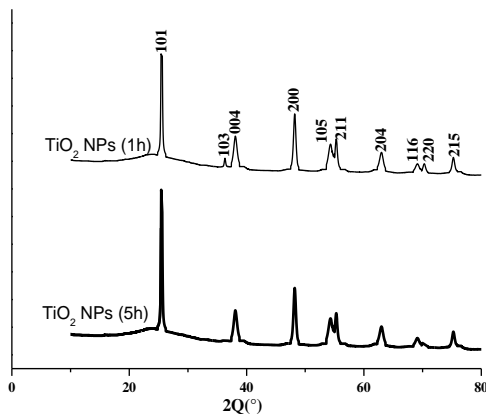


Fig. 2. X-ray diffraction (XRD) of  $\text{TiO}_2$  nanoparticles (NPs).

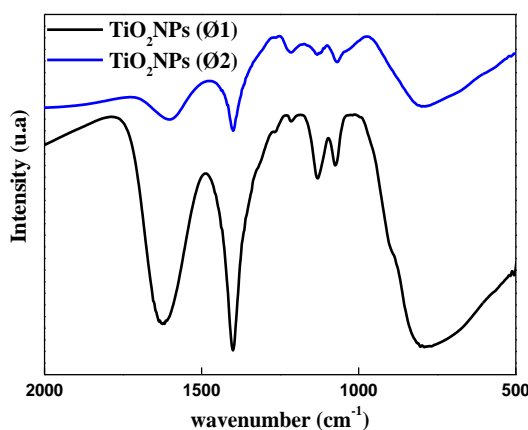


Fig. 3. Fourier transform-infrared spectroscopy (FT-IR) spectra of pure  $\text{TiO}_2$  NPs Ø1 (5h) and Ø2 (1h) samples.

a duration of 5 h can be attributed to higher precipitation intensity. The small size of NPs has an advantageous effect on their quantity, surface area, stiffening efficiency, and specific surface area [35].

The IR absorption spectrum of the material is shown in Fig. 3. The analysis of the spectrum shows a broad absorption peak in the range of  $800$  and  $450\text{ cm}^{-1}$ , which is attributed to the Ti-O vibration mode [34].

The surface morphology of the  $\text{TiO}_2$  NPs was examined using SEM. The SEM graph is shown in Fig. 4 (A and B) for  $\text{TiO}_2$  NPs. The SEM images revealed the presence of agglomerates of NPs and showed that the morphology is replete with spheres. Spherical particles showed better disintegration behavior and higher NP release in comparison to cylindrical particles upon contact with water [36]. A representative manually (ImageJ software) constructed histogram of particle size distribution of  $\text{TiO}_2$  is shown in Fig. 4 (C and D). The particle size of  $\text{TiO}_2$  NPs at  $500^\circ\text{C}$  for 1 h and 5 h were found to be 85 and 25 nm, respectively. The crystallite size obtained using Debye Scherrer formula is smaller than the particle size obtained by SEM. This is due to fact that the Debye Scherrer formula does not take into account the effect of lattice strain and instrumental factors on peak broadening.

#### Membrane characterization

##### Fourier Transform-Infrared (FT-IR) spectroscopy analysis

To confirm the effect of  $\text{TiO}_2$  NPs on the vibrational properties of membranes, IR spectroscopy was used since

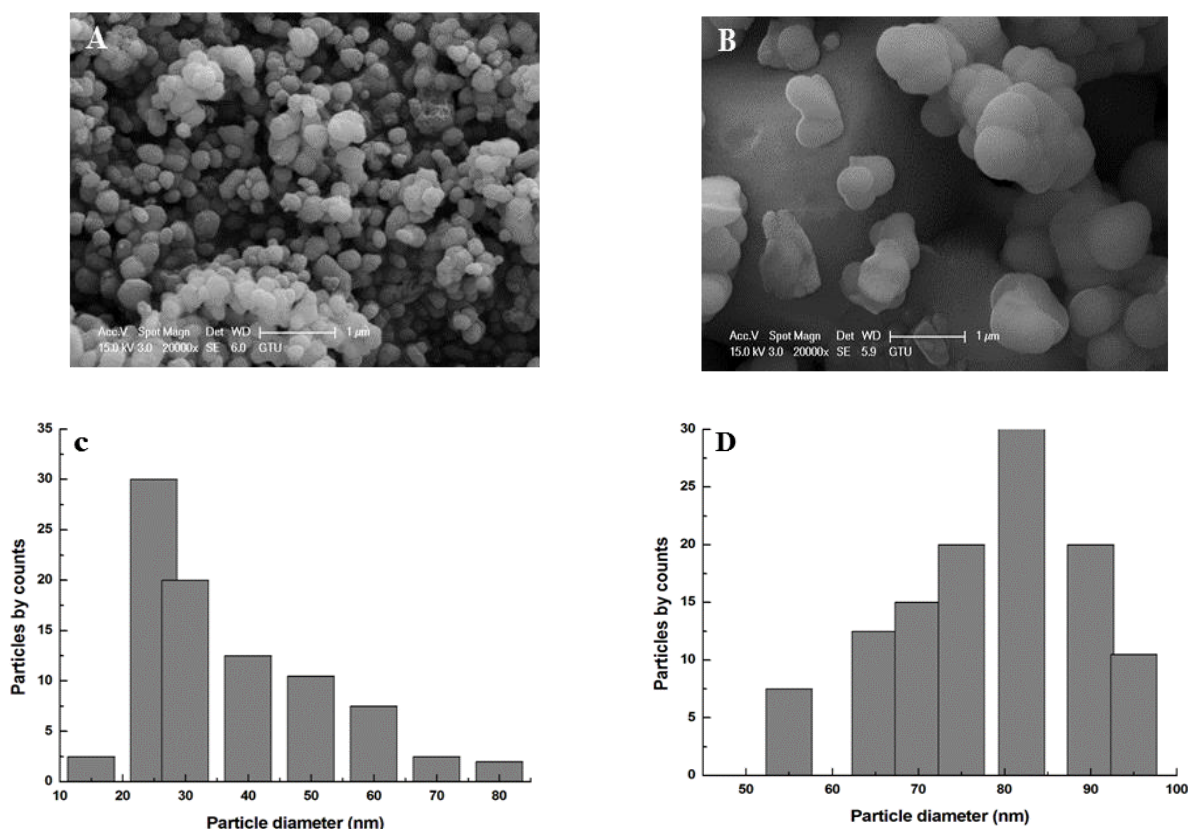


**Fig. 4:** Scanning electron microscope (SEM) image of TiO<sub>2</sub> nanoparticles (NPs) (A for NPs at Ø1, 23 nm and B for NPs at Ø2, 83 nm) × 20000 magnification and histogram of particle size distribution curve of TiO<sub>2</sub> NPs (C for NPs at Ø1, 23 nm and D for NPs at Ø2, 83 nm).

it is a very powerful characterization tool for identifying molecular groups and obtaining a wealth of microscopic information on their conformation and possible interactions. Fig. 5 shows the IR spectra of the membranes, with different TiO<sub>2</sub> compositions (M0, M1 and M2) recorded under the same conditions. TiO<sub>2</sub> was added as a modifier oxide. DMF and PEG 1000 are used as additives in the matrix (i.e., CA). The addition of TiO<sub>2</sub> is intended to improve the thermal properties, hardness, density of the membranes.

Based on the literature and the observation of the spectra of our samples, we noticed the appearance of a high intensity wide band located in the wave number range 2900-3500 cm<sup>-1</sup>. Such band could correspond to the stretching vibration of the hydroxyl groups [37]. The high intensity shoulder between 2971 and 2872 cm<sup>-1</sup> corresponds to the asymmetric and symmetric C-H stretching. We also observed a band that appears at 1744 cm<sup>-1</sup> corresponding to the vibration of the bonds (C=O) [38]. On the other hand, we noticed the appearance of a vibration located at

1638 cm<sup>-1</sup> and, which can be related to the distortion of the bond (O-H) due to water molecules. The low intensity bands that appear at 1218 cm<sup>-1</sup> are strongly related to the vibrations of carboxylate (C-O) groups [38].

In addition, the appearance of a band of medium intensity centered around 905 cm<sup>-1</sup> is related to the stretching vibrations Ti-O and the network O-Ti-O [39]. The Ti-O bond was of the TiO<sub>4</sub> (located at 740 cm<sup>-1</sup>) and TiO<sub>6</sub> (located at 650 cm<sup>-1</sup>) groups [40]. *Raghavaiah et al.* [41] are well resolved where it can be noted that the width of these two bands increased after the addition of TiO<sub>2</sub> NPs. We also noticed that the intensity of these bands (i.e., 740 cm<sup>-1</sup> and 650 cm<sup>-1</sup>) relative to M1 and M2 is remarkable, when compared with the M0 membrane. Further, after the addition of TiO<sub>2</sub> NPs, this band is shifted by 20 cm<sup>-1</sup> to the highest frequencies. The addition of TiO<sub>2</sub> also conducts to the appearance of an 873 cm<sup>-1</sup> shoulder due to vibrations of Ti-O-Ti bonds in TiO<sub>4</sub> entities, as it is reported in literature [42].

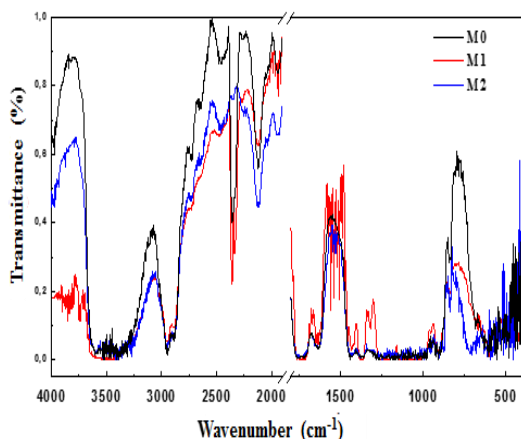


**Fig. 5:** Infrared (IR) spectrum of the bare and the nanocomposite membranes without TiO<sub>2</sub> nanoparticles (NPs) (M0), cellulose acetate (CA) membrane with TiO<sub>2</sub> NPs 23 nm (M1), CA membrane with TiO<sub>2</sub> NPs 83 nm (M2).

#### Scanning electron microscopy (SEM) analysis

SEM examination was used to assess the effectiveness of different TiO<sub>2</sub> NPs contents on the CA membrane. The morphology of CA membranes was investigated using SEM, and the resulting pictures of cross-section and top surface are shown in Fig. 6. CA membranes showed an asymmetrical morphology consisting of a dense layer supported on a porous sub-structure characterized by the presence of macro-voids, whereas both of the surfaces appeared uniform, smooth and dense. It is identified that the up-layers of the membranes restrict the flux and determine the rejection [43]. As seen in Fig. 6, by adding TiO<sub>2</sub> NPs (Ø1), the number of pores in the matrix membranes increases more than in the addition of TiO<sub>2</sub> NPs (Ø2). Also, in the sub-layer, the macro-void volume of all the modified membranes seems to be larger than the unfilled CA.

The aggregation of TiO<sub>2</sub> NPs is responsible for this discovery. Aggregation of NPs diminishes the effective surface of NPs, resulting in a decrease in the hydroxyl groups on the surface of modified membranes. These findings are consistent with prior researches [43,44]. Furthermore, several fractures can be seen on the surface of SEM pictures of TiO<sub>2</sub> NPs (Ø2) membrane. These cracks were most likely caused by the SEM imaging procedure, which revealed that the produced membrane was brittle due to the addition of TiO<sub>2</sub> NPs (Ø2) NPs. The comparison of the surface SEM images for TiO<sub>2</sub> NPs of different sizes showed that the dispersibility of Ø1 NPs

was the best and therefore led to the highest hydrophilicity for Ø1 embedded membranes [44].

#### Water contact angle measurement

Surface hydrophilicity is one of the important properties of membranes that can affect the flow and antifouling capacity of a membrane. As shown in Fig. 7, the contact angle of the incorporated membranes gradually decreases with the addition of TiO<sub>2</sub> NPs. The low angle of contact with water means high hydrophilicity, indicating that the addition of TiO<sub>2</sub> can improve the hydrophilicity of the membranes. However, the change in hydrophilicity may be related to the type of TiO<sub>2</sub>. The CA membrane had the highest water contact angle of  $92.64 \pm 1.5^\circ$ . By adding 0.05 g by weight of TiO<sub>2</sub>, the contact angle was reduced to  $49.7 \pm 0.7^\circ$  and  $86.7 \pm 0.2^\circ$  for TiO<sub>2</sub> NPs membranes (Ø1 and Ø2), respectively. The differences can be explained by considering the aggregation of TiO<sub>2</sub> NPs and their surface adsorbed -OH groups. In the M1 membrane, TiO<sub>2</sub> NPs have the lowest aggregation and largest adsorption -OH or adsorbed hydrophilicity. These parameters, low aggregation and high hydrophilicity, lead to a higher flow [44].

#### Water content and porosity study

The water content is related to the hydrophilic property of the membrane [45]. As shown in Fig. 8, the water content and porosity slightly increase by adding TiO<sub>2</sub> NPs. The separation of polymer chains due to the presence of TiO<sub>2</sub> NPs creates spaces in the polymer matrix that leads to an increase in water content. The porosity is little raised with the contribution of NPs in the membrane. It is well-known that high porosity promotes water flow. Increased exchange rates between water and solvent, as a general rule, can result in more porous membranes, and vice versa [43].

#### Water permeability

The CA and CA-composite membranes' performance was evaluated in terms of water permeability retention. Results of distilled water flux vs. pressure are displayed in Fig. 9, where a clear linear dependency of the flux with pressure is found, in accordance with Darcy's law. From the slope of such plot, the values of water permeability of the tested membranes could be determined:  $L_p^0(M0) = 9.4596 \text{ L/h.m}^2\text{.bar}$ ;  $L_p^0(M1) = 21.501 \text{ L/h.m}^2\text{.bar}$ ; and  $L_p^0(M2) = 7.1961 \text{ L/h.m}^2\text{.bar}$ . These permeabilities represent the initial state of the membranes and will be

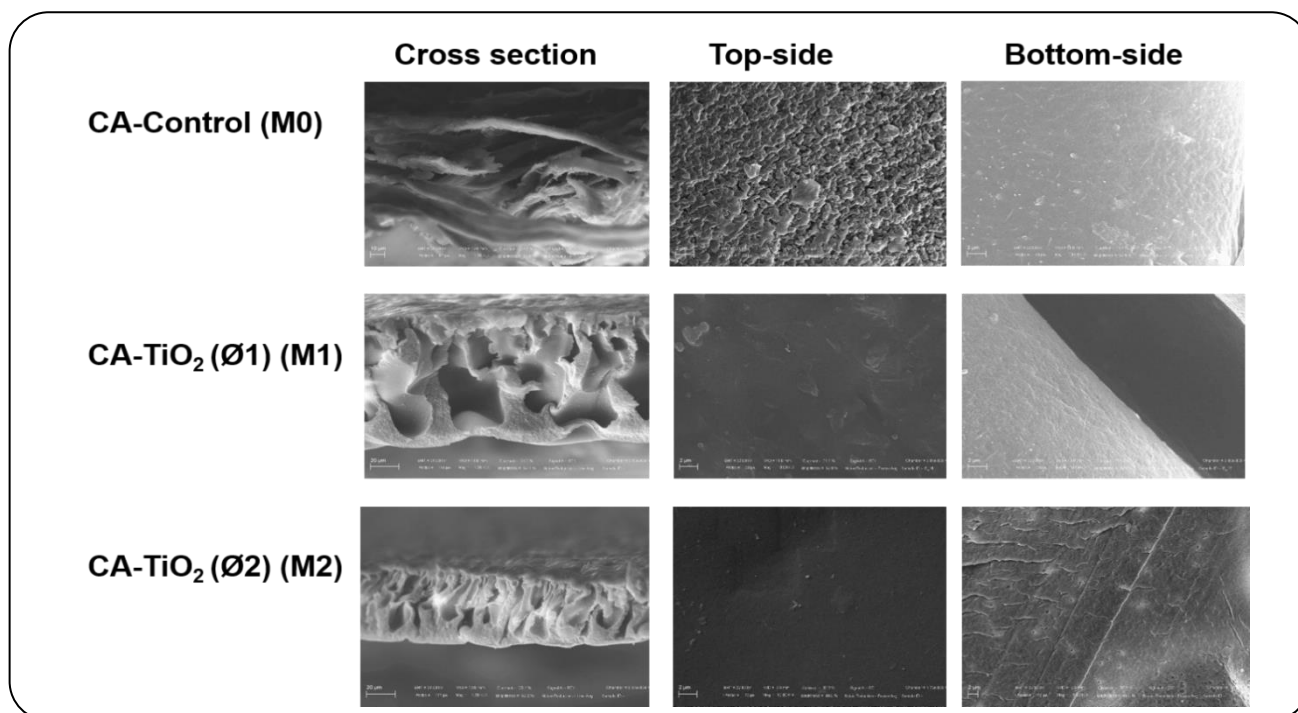


Fig. 6: Scanning electron microscopy (SEM) images of the bare and the nanocomposite membranes (Magnification of 1000 KX for cross section and 10000 KX and 5000 KX for top and bottom side, respectively).

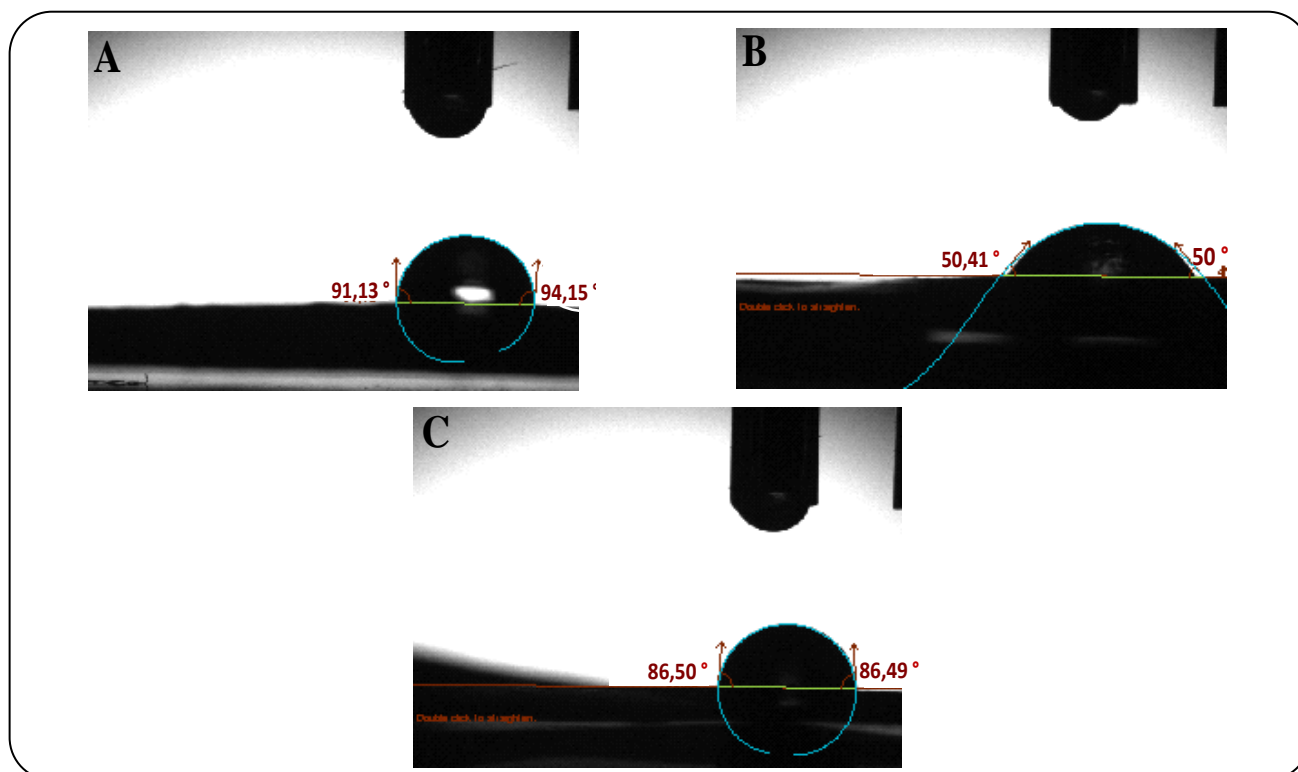
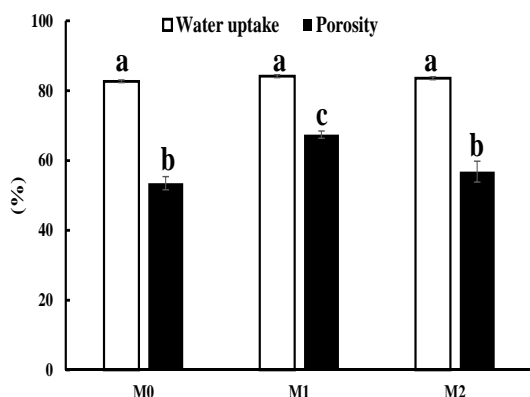
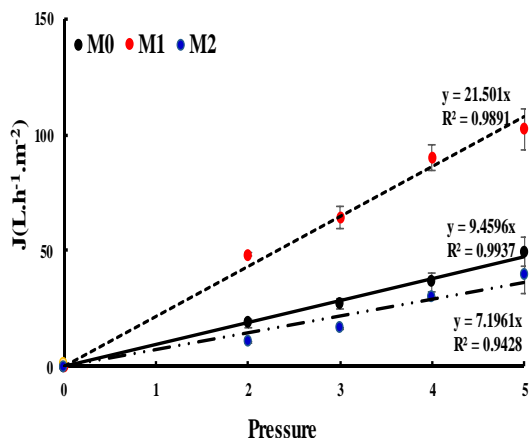


Fig. 7: Water contact angle of the bare and the nanocomposite membranes without TiO<sub>2</sub> nanoparticles (NPs) (A), cellulose acetate (CA) membrane with TiO<sub>2</sub> NPs 23 nm (B), CA membrane with TiO<sub>2</sub> NPs 83 nm (C).



**Fig. 8:** Water content and porosity measurements of the bare and the nanocomposite membranes without TiO<sub>2</sub> nanoparticles (NPs) (M0), cellulose acetate (CA) membrane with TiO<sub>2</sub> NPs 23 nm (M1), CA membrane with TiO<sub>2</sub> NPs 83 nm (M2). Data are means ( $\pm$  SE) of three replicates. Different letters represent significant differences between the treatment means. Differences were considered significant at  $p < 0.05$  level.



**Fig. 9:** Variation of pure water flux as a function of transmembrane pressure of cellulose acetate (CA) membrane without TiO<sub>2</sub> nanoparticles (NPs) (M0), CA membrane with TiO<sub>2</sub> NPs 23 nm (M1), CA membrane with TiO<sub>2</sub> NPs 83 nm (M2).

chosen as references. As expected, the flux increases linearly with the pressure, and the CA-composite membrane with TiO<sub>2</sub> NPs Ø1(M1) exhibited a higher flow than the pure membrane (M0). This phenomenon is due to the enhanced hydrophilicity and porosity of the membrane. These results reflect the SEM images and characterization analyzes findings. The CA composite membrane, which presented a higher permeability value, is strongly related

to its structure, having a thin selective layer and macrovoids. However, the membrane prepared from TiO<sub>2</sub> NPs Ø2 (M2) caused a decrease in the flow due to pore blockage caused by excess TiO<sub>2</sub> aggregation and also, due to its thicker elective layer [44].

### Filtration of dyes

#### Pressure effect

The effect of transmembrane pressure on the RR 180 (50 mg/L) retention and permeate flux was studied with  $\Delta P$  ranging from 2 to 5 bars. According to Fig. 10A, it is observed that the retention of RR 180 dye in the absence and presence of TiO<sub>2</sub> NPs remains independent of pressure. On the other hand, Fig. 10B shows that the permeate flux increases with pressure with the raising pressure. The data represent typical behavior for a driven pressure process. Increasing the pressure would force more water to pass through the membrane, which would lead to a higher permeate flux [46,47]. We also noted an important increase in permeate flux with the membrane CA/TiO<sub>2</sub> NPs (Ø1) (M1) and lower increase with the membrane CA/TiO<sub>2</sub> NPs (Ø2) (M2) compared to the reference membrane flux (M0). This is the result of partial clogging of the membrane pores by TiO<sub>2</sub> molecules of nominal diameter 83 nm [44].

#### Ionic strength effect

The presence of various compounds such as salts, acids and alkalis in textile dye effluent generally affects the efficiency of treatment processes such as adsorption or biological treatment. To study the effect of salinity on the efficiency of UF process, retention rate of RR 180 and permeate flux were monitored in presence of various concentrations of NaCl that was chosen as salt model. The concentration of NaCl was varied from 0.2 to 1 g/L, the concentration of dye fixed at 50 mg L<sup>-1</sup>, while the pressure was fixed at 3 bars. We observed in Fig. 11A that the retention rates of anionic dye RR 180 decreased with increasing NaCl concentration. It seems that the presence of a high concentration of NaCl induces a reduction in the electrostatic interaction between membrane surface containing several charged groups and the dye molecules. In other words, chloride ions compete with anionic dye in the complexation process between dye and CA [48,49]. It can be seen that the permeate flux is not dependent on NaCl concentration (Fig. 11B).

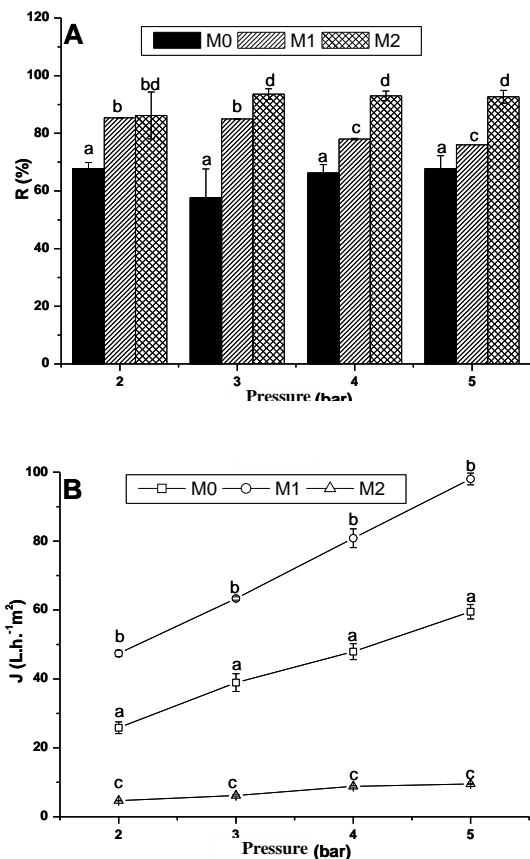


**Fig. 10:** (A) Transmembrane pressure effect on RR 180 dye retention and (B) permeate flux at  $C = 50$  ppm of cellulose acetate (CA) membrane without  $\text{TiO}_2$  nanoparticles (NPs) (M0), CA membrane with  $\text{TiO}_2$  NPs 23 nm (M1), CA membrane with  $\text{TiO}_2$  NPs 83 nm (M2). Data are means ( $\pm$  SE) of three replicates. Different letters represent significant differences between the treatment means. Differences were considered significant at  $p < 0.05$  level.

#### pH effect

The degree of ionization of the dye depends on the solution pH. This may affect the stability of the complex formed and thus the retention rate of the dye. In this study, the pH was varied from 2 to 10 by adding HCl or NaOH when the concentrations of dye were  $50 \text{ mg L}^{-1}$  and the transmembrane pressure was maintained at 3 bars. From Fig. 12 A, it is clearly observed that the RR 180 rejection values were in order of 96% for pH maintained between 2 and 4. Thereafter, from pH = 6, RR 180 removal decreases.

At pH = 10, for example, the retention rate of RR 180 is 67, 68 and 88% for M0, M1 and M2, respectively. This is why, it should be taken into account the electrostatic

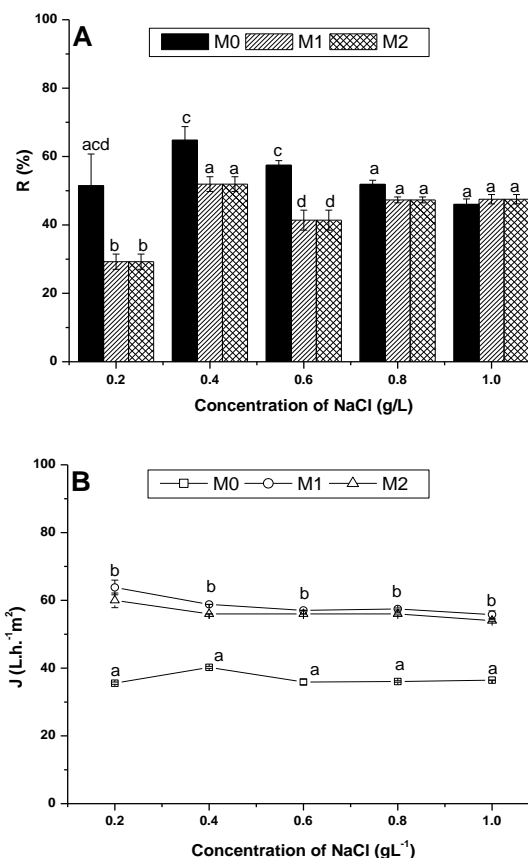


**Fig. 11:** (A) Salts effect on RR 180 dye retention and (B) permeate flux at  $\Delta P = 3$  bar and  $C = 50$  ppm of cellulose acetate (CA) membrane without  $\text{TiO}_2$  nanoparticles (NPs) (M0), CA membrane with  $\text{TiO}_2$  NPs 23 nm (M1), CA membrane with  $\text{TiO}_2$  NPs 83 nm (M2). Data are means ( $\pm$  SE) of three replicates. Different letters represent significant differences between the treatment means. Differences were considered significant at  $p < 0.05$  level.

interactions between membrane surface containing several charged groups and the dye molecules, which are also charged.

The membrane surface is expected to have a positive charge at  $\text{pH} < \text{pH}_{\text{PZC}}$ . However, at  $\text{pH} > \text{pH}_{\text{PZC}}$ , the surface should be negatively charged. The  $\text{pH}_{\text{PZC}}$  value for the CA membrane was found to be 5.3. At extreme values of pH, the change of pH after addition to the membrane is almost nil; however, there is a noticeable shift in sign in the pH increase in the intermediate range of pH, demonstrating that the overall charge of the membrane surface changes from negative to positive. The  $\text{pH}_{\text{PZC}}$  value for  $\text{TiO}_2$  NPs membrane was then determined to be 5.7, which is

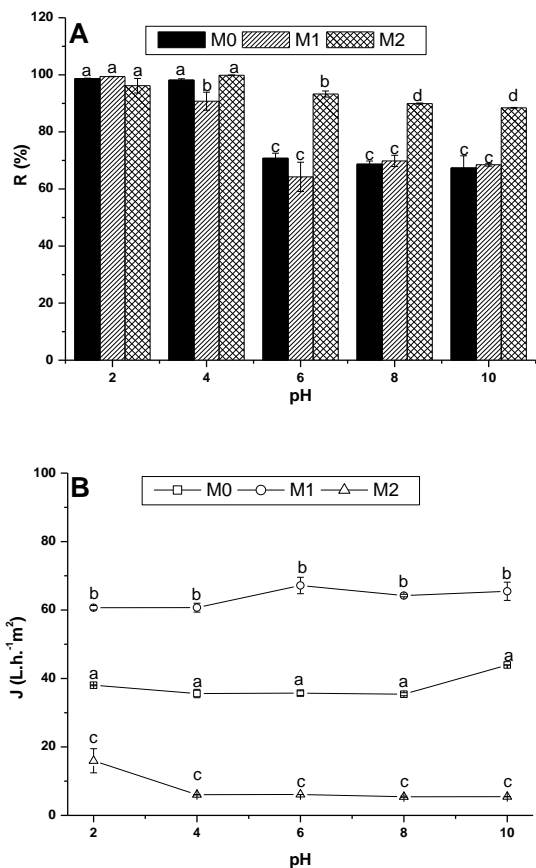


**Fig. 12:** (A) pH effect on RR 180 retention and (B) permeate flux at  $\Delta P = 3$  bar and  $C = 50$  ppm of cellulose acetate (CA) membrane without  $\text{TiO}_2$  nanoparticles (NPs) (M0), CA membrane with  $\text{TiO}_2$  NPs 23 nm (M1), CA membrane with  $\text{TiO}_2$  NPs 83 nm (M2). Data are means ( $\pm$  SE) of three replicates. Different letters represent significant differences between the treatment means. Differences were considered significant at  $p < 0.05$  level.

consistent with the value discovered by Bouazizi et al. [33]. At low pH values, the membrane presents a net positive charge while the dye molecules are negatively charged. This results in a strong attraction of dyes for the membrane surface where many of these dye molecules occupy possible adsorption sites. While the rest of the molecules pass freely through the pores, then leading to a low dye rejection. As pH increases, the membrane charge changes to negative and therefore the electrostatic interaction between membrane and solute molecules become repulsive, resulting in a clearly higher rejection of solutes. The same result was observed by Akbari et al. [50] and Seffaj et al. [51]. In the same context, there are studies on

the effect of zinc oxide (ZnO) and  $\text{TiO}_2$  NPs on supported lipid bilayers. Such studies demonstrated that through the variation in zeta potential (ZP) of ZnO with a pH of 7-8.5, the dispersions were found stable and positively charged (pH 7.4 and ZP  $\sim +3$  mV). Low ZPs tend to coagulate the ZnO suspension [52]. In variations of  $\text{TiO}_2$  ZP with a pH of 5 to 9, the dispersions are stable and the surface is positive (with a pH of 7.4, ZP = 33 mV). In this case, a high ZP will confer stability to  $\text{TiO}_2$ , i.e., the suspension resists to aggregation [53]. The effect of pH on permeate is also described. According to Fig. 12B, it is observed that the variation of the flux permeate of M1 is higher than that of M2. This difference can be linked to the pores of the M2 membrane that are partially blocked by  $\text{TiO}_2$  molecules of nominal diameter 83 nm.

#### Dye concentration effect

The influence of dye concentration on rejection and flux was studied by filtering the anionic dye at a constant pressure of 3 bar. The obtained results are shown in Fig. 13. The retention rate remains significantly unchanged for M0, while a significant decrease is noticed (45 and 79%) for M1 and M2, respectively. These findings indicate that  $\text{Ti}^{4+}$  ions compete with the dye molecules in the process of dye-CA complexation. Also, such results confirm that the NP-membrane interaction depends on the NP charge and ZP. Cationic NPs can penetrate through the membrane [53]. There is also an increase in the permeate flow with the  $\text{TiO}_2$ -membrane (M1) and one for reduction of the  $\text{TiO}_2$ -membrane (M2) compared to the reference membrane flow (M0). This is due to the narrowing of the pore diameters of the mixed membrane by  $\text{TiO}_2$  of nominal diameter 83 nm. Therefore, we can suppose that there are more effects leading to an increase of retention and decrease of flux. A possible explanation could be the presence of some dye molecules aggregation, being this aggregation more effective as the concentration of molecules increases [33,54]. Therefore, this initial rejection possibly could enhance the formation of a secondary polarization layer in the form of a gel, which plays an additional role of resistance to the permeation of dye molecules [55].

#### CONCLUSIONS

Cellulose Acetate (CA) membranes were created utilizing two different sizes of green synthesized  $\text{TiO}_2$  NPs.

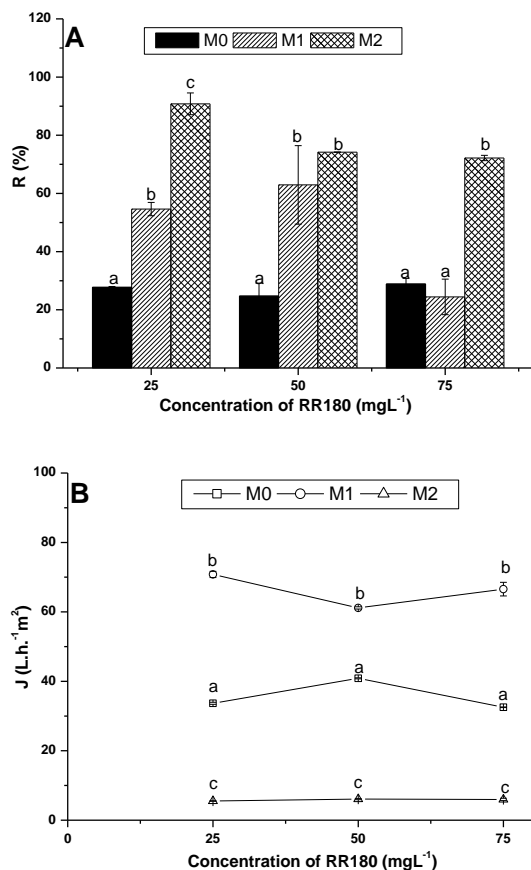


**Fig. 13.** (A) Rejection and (B) flux of the dye RR 180 as function of the concentration at  $\Delta P = 3$  bar of cellulose acetate (CA) membrane without  $\text{TiO}_2$  nanoparticles (NPs) (M0), CA membrane with  $\text{TiO}_2$  NPs 23 nm (M1), CA membrane with  $\text{TiO}_2$  NPs 83 nm (M2). Data are means ( $\pm$  SE) of three replicates. Different letters represent significant differences between the treatment means. Differences were considered significant at  $p < 0.05$  level.

The  $\text{TiO}_2$  ( $\emptyset 1$ ) nanoparticles (NPs) had low tendency to the aggregation and did not block the membrane pores that led to the higher pure water flux. The surface SEM images of the membranes showed that  $\text{TiO}_2$  NPs were aggregated by  $\text{TiO}_2$  ( $\emptyset 2$ ) mixed membranes, which caused membrane's pores clogging and reduced the pure water flux. The cross-section SEM images indicated that the size of macro-voids was reduced and the width of the membrane pores was slightly increased by the addition of  $\text{TiO}_2$  ( $\emptyset 1$ ). The dye retention could be, however, affected by the competitive effect of another chemical species present in solution such as NaCl salt. In the complexation process, chloride ions compete with anionic dye. Because of the contact force

between the membrane surface and the negatively charged anion of the RR 180, the retention rate was reduced at alkaline pH. An increase in permeate flow with membrane- $\text{TiO}_2$  ( $\emptyset 1$ ) compared to membrane- $\text{TiO}_2$  ( $\emptyset 2$ ) is explained by a partial blocking of the membrane's pores.  $\text{TiO}_2$  bio nanoparticle improves the performance of ultrafiltration and must be confronted with a real textile rejection to evaluate its efficacy.

#### Acknowledgements

This research has been funded by the Research Deanship of University of Ha'il, Saudi Arabia, through the Project RG-22 010.

Received : May 13, 2022 ; Accepted : Sep. 26, 2022

#### REFERENCES

- [1] Mahmood A., Recent Research Progress on Quasi-Solid-State Electrolytes for Dye-Sensitized Solar Cells, *J. Energy Chem.*, **24**(6): 686-692 (2015)
- [2] Mahmood A., Hussaintahir M., Irfan A., Computational Designing of Triphenylamine Dyes with Broad and Red-Shifted Absorption Spectra for Dye-Sensitized Solar Cells Using Multi-Thiophene Rings in  $\Pi$ -Spacer, *J. Comput. Electron.*, **36**(11): 2615-2620 (2015).
- [3] Mahmood A., & Khan S.U., Theoretical Designing of Novel Heterocyclic Azo Dyes for Dye Sensitized Solar Cells, *J. Comput. Electron.*, **13**: 1033-1041 (2014).
- [4] Samhaber W.M., Nguyen M.T., Applicability and Costs of Nanofiltration in Combination with Photocatalysis for the Treatment of Dye House Effluents, *Beistein J. Nanotechnol.*, **5**: 476-484 (2014).
- [5] Abedini R., Mahmoud S., Aminzadeh R., A Novel Cellulose Acetate (CA) Membrane Using  $\text{TiO}_2$  Nanoparticles: Preparation, Characterization and Permeation Study, *Desalination*, **277**(1-3): 40-45 (2011).
- [6] Abirami Saraswathia M.S.S., Ranab D., Alwarappanc S., Gowrishankard S., Kanimozhia P., Nagendrana A., Cellulose Acetate Ultrafiltration Membranes Customized with Bio-Inspired Polydopamine Coating and in Situ Immobilization of Silver Nanoparticles, *New J. Chem.*, **10** (2019).

- [7] Ferjani E., Lajimi R.H., Deratanib A., [Bulk and Surface Modification of Cellulose Diacetate Based RO/NF Membranes by Polymethylhydrosiloxane: Preparation and Characterization](#), *Desalination*, **146**: 325-330 (2002).
- [8] Qin J., Li Y., Lee L., Lee H., [Cellulose Acetate Hollow Fiber Ultrafiltration Membranes Made from CA/PVP 360 K/NMP/Water](#), *J. Membr. Sci.*, **218**: 173-183 (2003).
- [9] Sadrzadeh M., Saljoughi E., Shahidi K., [Preparation and Characterization of a Composite PDMS Membrane on CA Support](#), *Polym. Adv. Technol.*, **21(8)**: 568-577 (2010).
- [10] Zularisam A.W., Ismail A.F., Salim M.R., Sakinah M., Ozaki H., [The Effects of Natural Organic Matter \(NOM\) Fractions on Fouling Characteristics and Flux Recovery of Ultrafiltration Membranes](#), *Dessalination*, **212**: 191-208 (2007).
- [11] Roelofs K.S., Hirth T., Schiestel T., [Sulfonated Poly \(Ether Ether Ketone\)-Based Silica Nanocomposite Membranes for Direct Ethanol Fuel Cells](#), *J. Membr. Sci.*, **346**: 215-226 (2010).
- [12] Huang Z., Chen K., Li S., Yin X., Zhang Z., Xu H., [Effect of ferrosulfate Oxide Content on the Performances of Polysulfone-Ferrosulfate Oxide Ultrafiltration Membranes](#), *J. Membr. Sci.*, **315**: 164-171(2008).
- [13] Darvishmanesh S., Buekenhoudt A., Degreè J., Bruggen B.V.D., [General Model for Prediction of Solvent Permeation Through Organic and Inorganic Solvent Resistant Nanofiltration Membranes](#), *J. Membr. Sci.*, **334**: 43-49 (2009).
- [14] Yan L., Shui Y., Bao C., [Preparation of Poly \(vinylidene fluoride\)\(PVDF\) Ultrafiltration Membrane Modified by Nano-Sized Alumina \(Al<sub>2</sub>O<sub>3</sub>\) and Its Antifouling Research](#), *Polymer*, **46**: 7701-7706 (2005).
- [15] Li J., Xu Z., Yang H., Yu L., Liu M., [Effect of TiO<sub>2</sub> Nanoparticles on the Surface Morphology and Performance of Microporous PES Membrane](#), *Appl. Surf. Sci.*, **255**: 4725-4732 (2009).
- [16] Ahn J., Chung W., Pinnau I., Guiver M.D., [Polysulfone/Silica Nanoparticle Mixed-Matrix Membranes for Gas Separation](#), *J. Membr. Sci.*, **314**: 123-133 (2008).
- [17] Kim J., Bruggen B. Van Der., [The Use of Nanoparticles in Polymeric and Ceramic Membrane Structures: Review of Manufacturing Procedures and Performance Improvement for Water Treatment](#), *Environ. Pollut.*, **158(7)**: 2335-2349 (2010).
- [18] Li J., Zhu J., Zheng M., [Morphologies and Properties of Poly \(phthalazinone ether sulfone ketone\) Matrix Ultrafiltration Membranes with Entrapped TiO<sub>2</sub> Nanoparticles](#), *J. Appl. Polym. Sci.*, **103(6)**: 3623-3629 (2006).
- [19] Xu Z., Yu L., Han L., [Polymer-Nanoinorganic Particles Composite Membranes: A Brief Overview](#), *Front. Chem. Eng.*, **3(3)**: 318-329 (2009).
- [20] Razmjou A., Mansouri J., Chen V., [The Effects of Mechanical and Chemical Modification of TiO<sub>2</sub> Nanoparticles on the Surface Chemistry, Structure and Fouling Performance of PES Ultrafiltration Membranes](#), *J. Membr. Sci.*, **378(1-2)**: 73-84 (2011).
- [21] Chung T., Ying L., Li Y., Kulprathipanja S., [Mixed Matrix Membranes \(MMMs\) comprising Organic Polymers with Dispersed Inorganic Fillers for Gas Separation](#), *Prog. Polym. Sci.*, **32**: 483-507 (2007).
- [22] Madaeni S.S., Ghaemi N., Alizadeh A., Joshaghani M., [Influence of Photo-Induced Superhydrophilicity of Titanium Dioxide Nanoparticles on the Anti-Fouling Performance of Ultrafiltration Membranes](#), *Appl. Surf. Sci.*, **257(14)**: 6175-6180 (2011).
- [23] Mansourpanah Y., Madaeni S.S., Rahimpour A., Farhadian A., Taheri A.H., [Formation of Appropriate Sites on Nanofiltration Membrane Surface for Binding TiO<sub>2</sub> Photo-Catalyst: Performance , Characterization and Fouling-Resistant Capability](#), *J. Membr. Sci.*, **330**: 297-306 (2009).
- [24] Nasir A.M., Goh P.S., Ismail A.F., [Synthesis Route for the Fabrication of Nanocomposite Membranes](#), *Micro and Nano Technol., Elsevier Inc.*, 69-89 (2020).
- [25] Younas H., Ur Z., Afridi R., Zhou Y., Cui Z., [Progress and Perspective of Antifouling, Pressure Driven, Flat-Sheet Nanocomposite, Polymeric Membranes in Water Treatment](#), *J. Membr. Sci. Res. J.*, **6**: 319-332 (2020).
- [26] Campiglio C.E., Negrini N.C., Far S., Draghi L., [Cross-Linking Strategies for Electrospun Gelatin Scaffolds](#), *Materials*, **12(15)**: 2476 (2019).
- [27] Chu J.Y., Lee K.H., Kim A.R., Yoo D.J., [Improved Electrochemical Performance of Composite Anion Exchange Membranes for Fuel Cells Through Cross Linking of the Polymer Chain with Functionalized Graphene Oxide](#), *J. Membr. Sci.*, **611(1)**: 118385 (2020).

- [28] Singh A., Gautam P.K., Verma A., Singh V., Shivapriya P.M., Shivalkar S., Samanta S.K., Green Synthesis of Metallic Nanoparticles as Effective Alternatives to Treat Antibiotics Resistant Bacterial Infections: A Review, *Biotechnol. Rep.*, **25**: e00427 (2020).
- [29] Rao K.G., Ashok C.H., Rao V., Chakra C.H.S., Tambur P., Green Synthesis of TiO<sub>2</sub> Nanoparticles Using *Aloe vera* Extract, *Int. J. Adv. Res. Phys. Sci.*, **2**: 28-34 (2015).
- [30] Sethy N.K., Arif Z., Mishra P.K., Kumar P., Green Synthesis of TiO<sub>2</sub> Nanoparticles from *Syzygium cumini* Extract for Photo-Catalytic Removal of Lead (Pb) in Explosive Industrial Wastewater, *Green Process. Synth.*, **9**: 171-181 (2020).
- [31] Liguó S., Xiaokai B., Xiaofeng L., Liuqing S., Zhongying L., Lifang C., Zhengchi H., Kai Fan., Preparation and Characterization of ZnO/Polyethersulfone (PES) Hybrid Membranes, *Desalination*, **293**: 21-29 (2012).
- [32] Ursino C., Nicolò E.D., Gabriele B., Criscuoli A., Figoli A., Development of a novel Perfluoropolyether (PFPE) Hydrophobic/Hydrophilic Coated Membranes for Water Treatment, *J. Membr. Sci.*, **581**(1): 58-71 (2019).
- [33] Bouazizi A., Breida M., Achiou B., Ouammou M., Removal of Dyes by a New Nano-TiO<sub>2</sub> Ultrafiltration Membrane Deposited on Low-Cost Support Prepared from Natural Moroccan Bentonite, *Appl. Clay Sci.*, **148**(1): 127-135 (2017).
- [34] Missaoui T., Smiri M., Chmingui H., Hafiane A., Effects of Nanosized Titanium Dioxide on the Photosynthetic Metabolism of Fenugreek (*Trigonella foenum-graecum* L.), *C.R. Biol.*, **340**(11,12): 453-564 (2017).
- [35] Ashraf M.A., Peng W., Zare Y., Rhee K.Y., Effects of Size and Aggregation/Agglomeration of Nanoparticles on the Interfacial/Interphase Properties and Tensile Strength of Polymer Nanocomposites, *Nanoscale Res. Lett.*, **13**: 214 (2018).
- [36] Torge A., Pavone G., Jurisic M., Lima-engelmann K., A Comparison of Spherical and Cylindrical Microparticles Composed of Nanoparticles for Pulmonary Application, *Aerosol Sci. Technol.*, **53**(1): 53-62 (2019).
- [37] Neelapala S.D., Nair A.K., Jagadeeshbabu P.E., Synthesis and Characterisation of TiO<sub>2</sub> Nanofibre/Cellulose Acetate Nanocomposite Ultrafiltration Membrane, *J. Exp. Nanosci.*, **12**(1): 152-165 (2017).
- [38] Abdel-naby A.S., Al-ghamdi A.A., Chemical Modification of Cellulose Acetate by N-( phenyl amino) Maleimides: Characterization and Properties, *Int. J. Biol. Macromol.*, **68**: 21-27 (2014).
- [39] Golobostanfard M.R., Abdizadeh H., Effects of Acid Catalyst Type on Structural, Morphological, and Optoelectrical Properties of Spin-Coated TiO<sub>2</sub> Thin Film, *Phys. B*, **413**(15): 40-46 (2013).
- [40] Ra, R.B., Rao D.K., Veeraiah N., The Role of Titanium Ions on Structural, Dielectric and Optical Properties of Li<sub>2</sub>O-MgO-B<sub>2</sub>O<sub>3</sub> Glass System, *Mater. Chem. Phys.*, **87**: 357-369 (2004).
- [41] Raghavaiah B.V., Laxmikanth C., Veeraiah N., Spectroscopic Studies of Titanium Ions in PbO-Sb<sub>2</sub>O<sub>3</sub>-As<sub>2</sub>O<sub>3</sub> Glass System, *Opt. Commun.*, **235**: 341-349 (2004).
- [42] Fukushima T., Benino Y., Fujiwara T., Dimitrov V., Komatsu T., Electronic Polarizability and Crystallization of K<sub>2</sub>O-TiO<sub>2</sub>-GeO<sub>2</sub> Glasses with High TiO<sub>2</sub> Contents, *J. Solid State Chem.*, **179**(12): 3949-3957 (2006).
- [43] Alhalili Z., Romdhani C., Chemingui H., Smiri M., Removal of Dithieterthiol (DTT) from Water by Membranes of Cellulose Acetate (CA) and CA Doped ZnO and TiO<sub>2</sub> Nanoparticles, *J. Saudi Chem. Soc.*, **25**(8): 101282 (2021).
- [44] Vatanpour V., Siavash S., Reza A., Salehi E., Zinadini S., Ahmadi H., TiO<sub>2</sub> Embedded Mixed Matrix PES Nanocomposite Membranes: Influence of Different Sizes and Types of Nanoparticles on Antifouling and Performance, *Desalination*, **292**: 19-29 (2012).
- [45] Hosseini S.M., Karami F., Farahani S.K., Bandehali S., Shen J., Bagheripour E., Seidy-poor A., Tailoring the Separation Performance and Antifouling Property of Polyethersulfone Based NF Membrane by Incorporating Hydrophilic CuO Nanoparticles, *Korean J. Chem. Eng.*, **37**(5): 866-874 (2020).
- [46] Hammami M., Ennigrou D.J., Horchani-naifer K., Ferid M., Comparative Study of Neodymium Recovery from Aqueous Solutions by Polyelectrolytes Assisted-Ultrafiltration, *Korean J. Chem. Eng.*, **34**(7): 1-8 (2017).

- [47] Mondal S., Ouni H., Dhahbi M., De S., [Kinetic Modeling for Dye Removal Using Polyelectrolyte Enhanced Ultrafiltration](#), *J. Hazard. Mater.*, **229-230**: 381-389 (2012).
- [48] Sorlier P., Denuzie A., Viton C., Domard A., [Relation between the Degree of Acetylation and the Electrostatic Properties of Chitin and Chitosan](#), *Biomacromolecules*, **2**: 765-772 (2001).
- [49] Fradj A., Ben Hamouda S.B., Ouni H., Lafi R., Gzara L., Hafiane A., [Removal of Methylene Blue from Aqueous Solutions by Poly \(Acrylic Acid\) and Poly \(Ammonium Acrylate\) Assisted Ultrafiltration](#), *Sep. Purif. Technol.*, **133(8)**: 76-81 (2014).
- [50] Akbari A., Remigy J.C., Aptel P., [Treatment of Textile Dye Effluent Using A Polyamide-Based Nanofiltration Membrane](#), *Chem. Eng. Process.*, **41**: 601-609 (2002).
- [51] Seffaj N., Younsi S.A., Persin M., Cretin M., [Processing and Characterization of TiO<sub>2</sub>/ ZnAl<sub>2</sub>O<sub>4</sub> Ultrafiltration Membranes Deposited on Tubular Support Prepared from Moroccan Clay](#), *Ceram. Int.*, **31**: 205-210 (2005).
- [52] Metka Š., Dra B., Vid Š., Zupanc J., Roman Š., Makovec D., Erdogmus D., [Effect of Engineered TiO<sub>2</sub> and ZnO Nanoparticles on Erythrocytes, Platelet-Rich Plasma and Giant Unilamellar Phospholipid Vesicles](#), *BMC Vet. Res.*, **9(7)**: 3-13 (2013).
- [53] Heikkilä, E., Martinez-Seara, H., Gurtovenko, A.A., Vattulainen, I., Akola, J., [Atomistic Simulations of Anionic Au<sub>144</sub>\(SR\)<sub>60</sub> Nanoparticles Interacting with Asymmetric Model Lipid Membranes](#), *Biochim. Biophys. Acta - Biomembr.*, **1838(11)**: 2852-2860 (2014).
- [54] Lin J., Ye W., Baltaru M., Tang Y.P., Bernstein N.J., Gao P., Balta S., Vlad M., Volodin A., Sotto A., Luis P., Zydney A.L., Der Bruggen B.V., [Tight Ultrafiltration Membranes for Enhanced Separation of Dyes and Na<sub>2</sub>SO<sub>4</sub> During Textile Wastewater Treatment](#), *J. Membr. Sci.*, **514(15)**: 217-228 (2016).
- [55] Yu S., Chen Z., Cheng Q., Lü Z., Liu M., Gao C., [Application of Thin-Film Composite Hollow Fiber Membrane to Submerged Nanofiltration of Anionic Dye Aqueous Solutions](#), *Sep. Purif. Technol.*, **88**: 121-129 (2012).